Experimental Section

Synthesis of $FeVO_4$ porous nanorods

All the chemicals are of analytical grade and used as received. Briefly, 0.1 M $Fe(NO_3)_3 \cdot 6H_2O$ was dissolved in 30 mL de-ionized water, to which 0.1 M NH_4VO_3 was added under magnetic stirring. The mixed solution was sealed in a Teflon-lined stainless steel autoclave and maintained in the oven at 160 °C for 3 h. The resulting precipitates were collected via centrifugation and further washed with distilled water and ethanol several times. After that, the dried precipitates were placed in a muffle furnace and calcined in air at 500 ^oC for 6 h to obtain $FeVO_4$ porous nanorods.

Characterizations

X-ray diffraction (XRD) pattern was recorded on a Rigaku D/max 2400 diffractometer. Transmission electron microscopy (TEM), high-resolution transmission electron microscopy (HRTEM) were performed on a Tecnai G^2 F20 microscope. X-ray photoelectron spectroscopy (XPS) analysis was conducted on a PHI 5702 spectrometer. Nitrogen adsorption/desorption isotherms were recorded on an ASAP 2020 instrument. ^1H nuclear magnetic resonance (NMR) measurements were performed on a 500 MHz Bruker superconducting-magnet NMR spectrometer. Prior to NMR measurements, all the feeding gases were respectively purified by an acid trap (0.05 M H_2SO_4) to eliminate the potential NO_x and NH_3 contaminants[1].

Electrochemical measurements

Electrochemical measurements were conduced on a CHI-660E electrochemical workstation using a three-electrode system consisting of counter electrode (graphite

rod), working electrode (CC sample) and reference electrode (Ag/AgCl). All potentials were referenced to a reversible hydrogen electrode (RHE) by E_{RHE} (V) = $E_{Ag/AgCl}$+0.197+0.059×pH. The CC (1 × 1 cm^2) was pretreated by soaking it in 0.5 M H_2SO_4 for 12 h, and then washed with deionized water several times and dried at 60 ^oC for 24 h. The working electrode was fabricated by depositing 20 μL of the catalyst ink onto the pretreated CC (0.2 mg cm^{-2}) and dried in the air. The catalyst ink was fabricated by ultrasonically dispersing 1 mg of the catalyst in 100 μL of ethyl alcohol containing 5 μL of Nafion (5 wt%). The NRR tests were carried out in an H-type two-compartment electrochemical cell separated by a Nafion 211 membrane [2-4]. The Nafion membrane was pretreated by boiling it in 5% H_2O_2 solution for 1 h, 0.5 M H_2SO_4 for 1 h and deionized water for 1 h in turn. During each electrolysis, ultra-high-purity N_2 gas (99.999%) was continuously purged into the cathodic chamber at a flow rate of 20 mL min^{-1}. After each NRR electrolysis, the produced NH_3 and possible N_2H_4 were quantitatively determined by the indophenol blue method[5], and approach of Watt and Chrisp[6], respectively.

Determination of NH_3

Typically, 4 mL of electrolyte was removed from the electrochemical reaction vessel. Then 50 μL of solution containing NaOH (0.75 M) and NaClO (ρ_{Cl} = ~4.5), 500 μL of solution containing 0.32 M NaOH, 0.4 M $C_7H_6O_3Na$, and 50 μL of $C_5FeN_6Na_2O$ solution (1 wt%) were respectively added into the electrolyte. After standing for 2 h, the UV-vis absorption spectrum was measured and the concentration-absorbance curves were calibrated by the standard NH_4Cl solution with

a series of concentrations.

NH_3 yield was calculated by the following equation:

$$\mathrm{NH_3\ yield}\ (\mu g\ h^{-1}\ mg_{cat.}^{-1}) = \frac{c_{NH_3} \times V}{t \times m} \quad (1)$$

Faradaic efficiency was calculated by the following equation:

$$\text{Faradaic efficiency}\ (\%) = \frac{3 \times F \times c_{NH_3} \times V}{17 \times Q} \times 100\% \quad (2)$$

where c_{NH3} (μg mL^{-1}) is the measured NH_3 concentration, V (mL) is the volume of the electrolyte, t (h) is the reduction time and m (mg) is the mass loading of the catalyst on CC. F (96500 C mol^{-1}) is the Faraday constant, Q (C) is the quantity of applied electricity.

Determination of N_2H_4

Typically, 5 mL of electrolyte was removed from the electrochemical reaction vessel. The 330 mL of color reagent containing 300 mL of ethyl alcohol, 5.99 g of $C_9H_{11}NO$ and 30 mL of HCl were prepared, and 5 mL of color reagent was added into the electrolyte. After stirring for 10 min, the UV-vis absorption spectrum was measured and the concentration-absorbance curves were calibrated by the standard N_2H_4 solution with a series of concentrations.

Calculation details

DFT computations were carried out by using the Cambridge sequential total energy package (CASTEP)[7]. The projector augmented wave (PAW) pseudopotential with the Perdew–Burke–Ernzerhof (PBE) exchange-correlation function was utilized in the calculations. To ensure all atoms were fully relaxed for

each system, the convergence tolerance was set as 1.0×10^{-5} eV for energy and 0.02 eV $Å^{-1}$ for force. The 4×4×1 Monkhorst-Pack mesh was used in Brillouin zone sampling. The kinetic cutoff energy for the plane wave basis was set at 500 eV. The $FeVO_4$ (120) slab was modeled by a 2×2 supercell and a vacuum region of 15 Å was used to separate adjacent slabs. To sufficiently consider the on-site Columbic repulsion between the d electrons, the Hubbard *U* corrections were applied to transition metal d-electrons and the values of *U*–*J* parameters for Fe (2.0) and V (3.2) atoms were adopted [8].

The Gibbs free energy (ΔG, 298 K) of reaction steps is calculated by [9]:

$$\Delta G=\Delta E+\Delta ZPE-T\Delta S \quad (3)$$

where ΔE is the adsorption energy, ΔZPE is the zero point energy difference and $T\Delta S$ is the entropy difference between the gas phase and adsorbed state. The entropies of free gases were acquired from the NIST database.

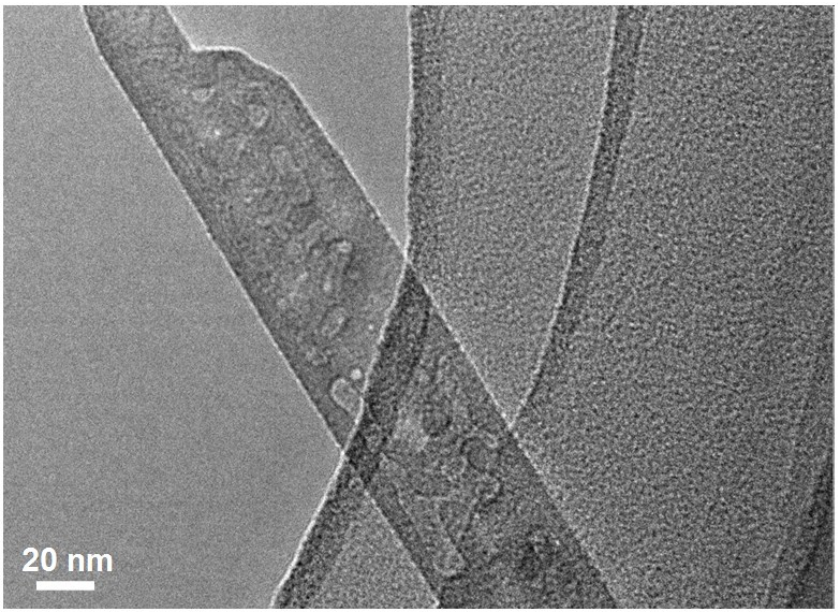

Fig. S1. TEM image of $FeVO_4$ PNRs.

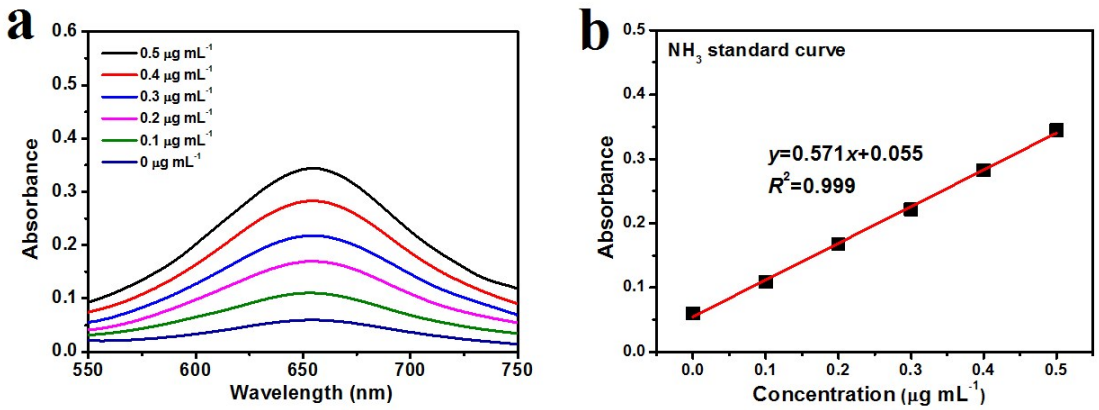

Fig. S2. (a) UV-Vis absorption spectra of indophenol assays with NH_4Cl after incubated for 2 h at ambient conditions. (b) Calibration curve used for calculation of NH_3 concentrations.

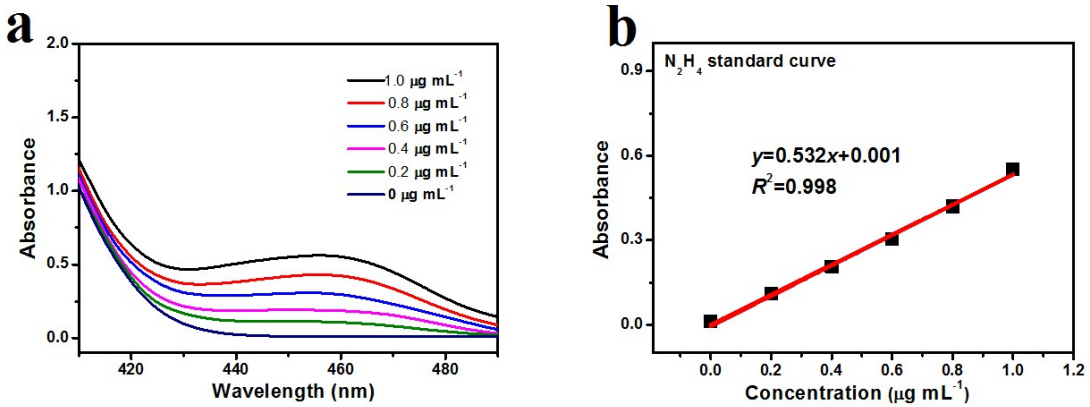

Fig. S3. (a) UV-Vis absorption spectra of N_2H_4 assays after incubated for 20 min at ambient conditions. (b) Calibration curve used for calculation of N_2H_4 concentrations.

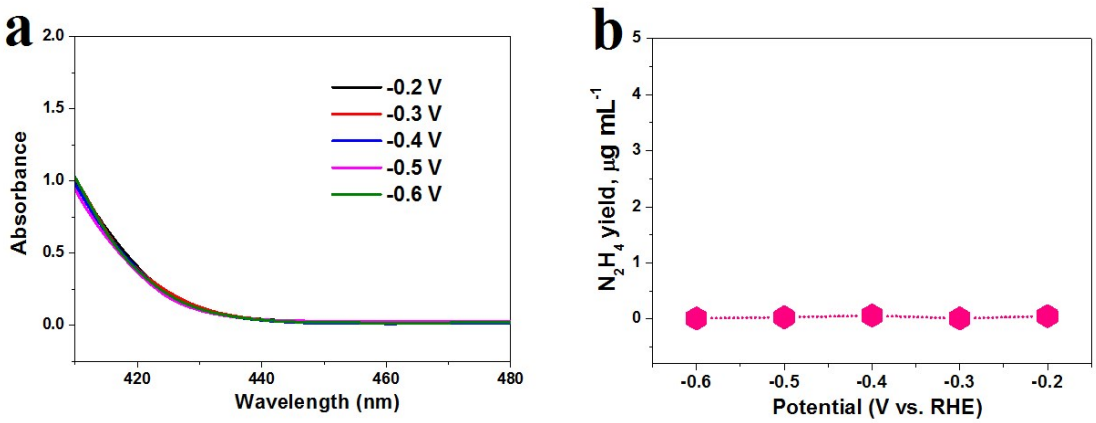

Fig. S4. (a) UV-Vis spectra of the electrolytes (stained with the chemical indicator based on the method of Watt and Chrisp) after 2 h of electrocatalysis on $FeVO_4$ PNRs at various potentials, and (b) corresponding N_2H_4 concentrations in the electrolytes.

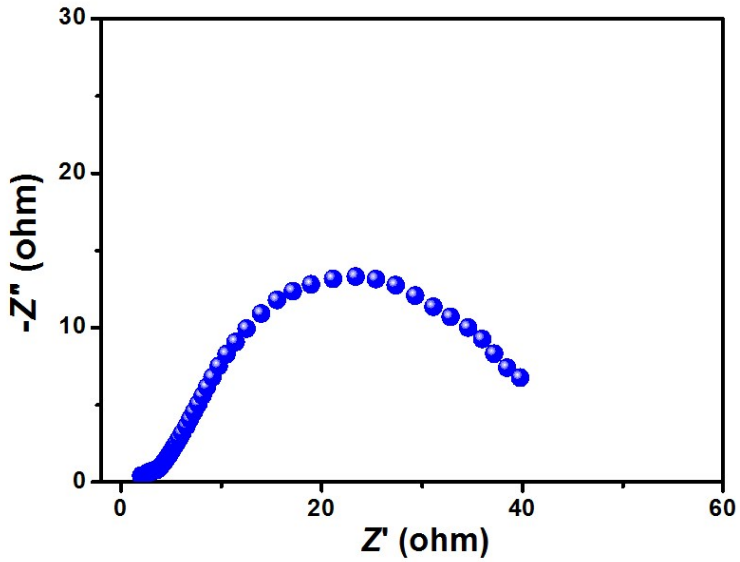

Fig. S5. Electrochemical impendence spectra of $FeVO_4$ PNRs.

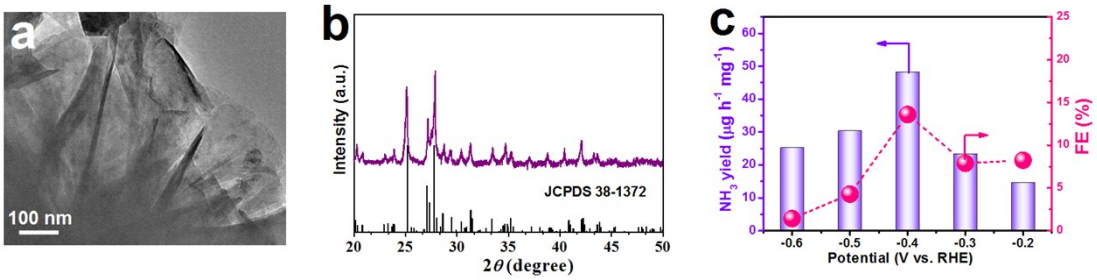

Fig. S6. (a) TEM image of $FeVO_4$ nanosheets prepared by a reported method[10]. (b) XRD pattern of $FeVO_4$ nanosheets. (c) NH_3 yield/FE data of $FeVO_4$ nanosheets.

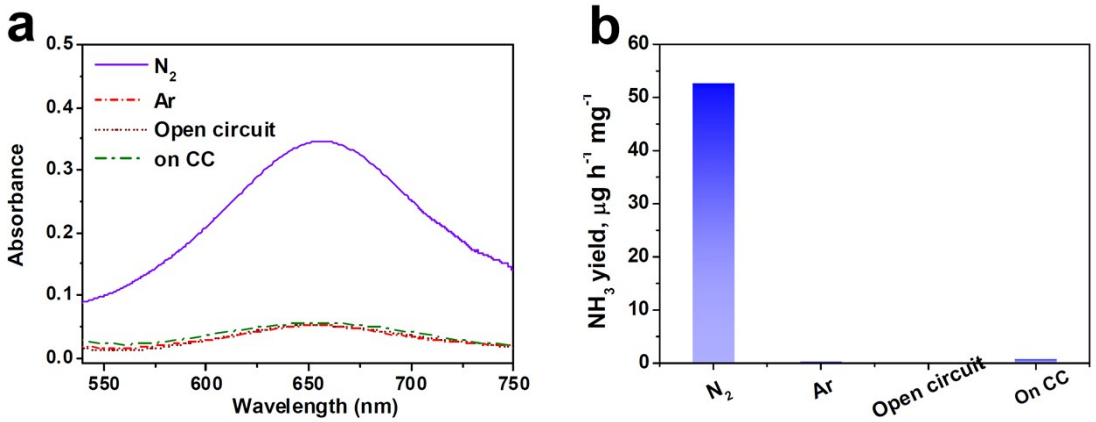

Fig. S7. (a) UV-Vis absorption spectra of the electrolytes stained with indophenol indicator after 2 h electrolysis on $FeVO_4$ PNRs at -0.4 V in N_2-saturated solution, Ar-saturated solutions, N_2-saturated solution at open circuit and N_2-saturated solution on pristine CC, and (b) corresponding NH_3 yields.

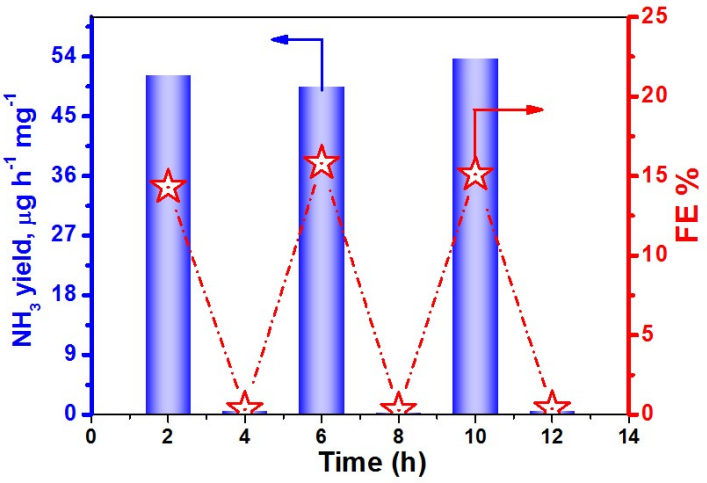

Fig. S8. Alternating cycling test of $FeVO_4$ PNRs by switching electrolysis between Ar-saturated and N_2-saturated solutions for 12 h at −0.4 V.

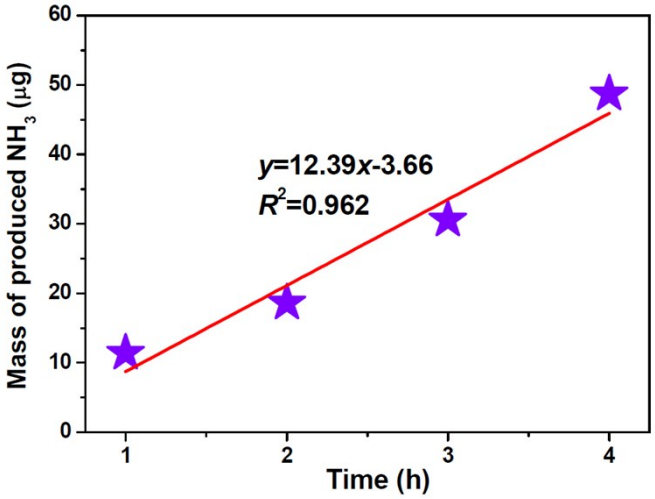

Fig. S9. Mass of produced NH_3 after electrolysis at various times on $FeVO_4$ PNRs.

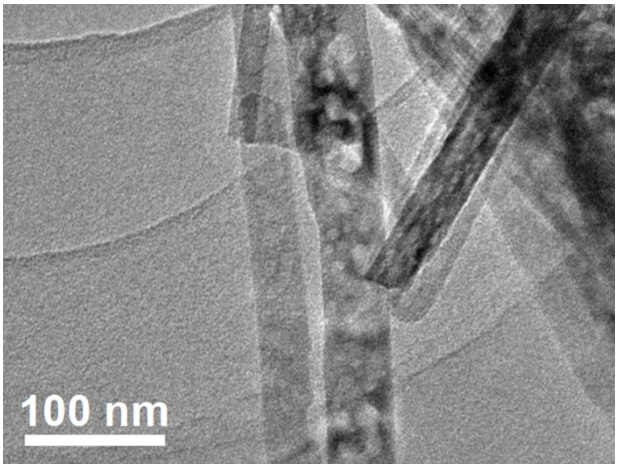

Fig. S10. TEM image of $FeVO_4$ PNRs after stability test.

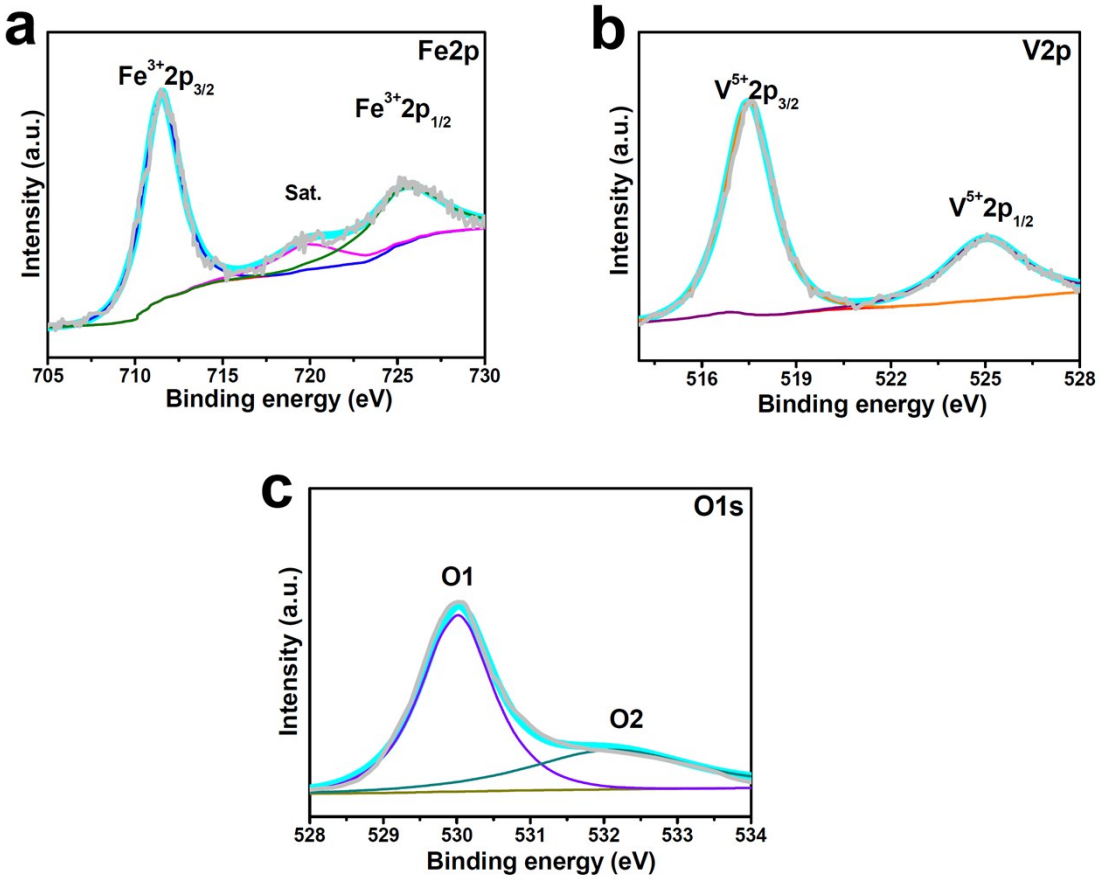

Fig. S11. XPS spectra of $FeVO_4$ PNRs (scraped down from CC) after stability test: (a) Fe2p; (b) V2p; (c) O1s.

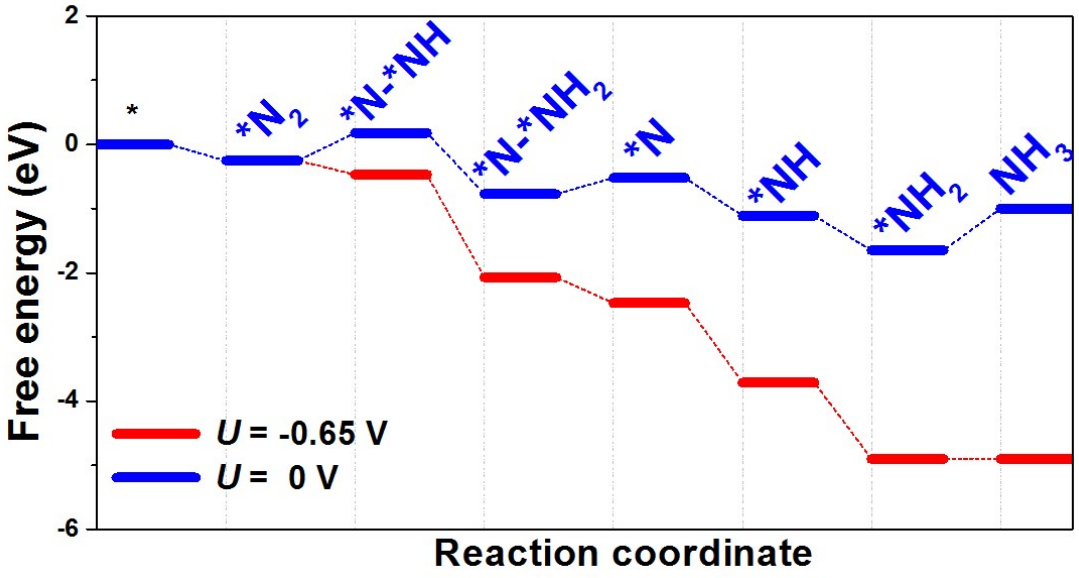

Fig. S12. Free energy diagrams of consecutive NRR pathway on Fe_{2c}-V_{2c} dimer at zero and applied energy of -0.65 V.

Table S1. Comparison of optimum NH_3 yield and Faradic efficiency (FE) for recently reported state-of-the-art NRR electrocatalysts at ambient conditions

Catalyst	Electrolyte	Determination method	Optimum Potential (V Vs RHE)	NH_3 yield ($\mu g\ h^{-1}\ mg^{-1}$)	FE (%)	Ref.
$Bi_4V_2O_{11}$-CeO_2 nanofibers	0.1 M HCl	Indophenol blue method	-0.2	23.21 $\mu g\ h^{-1}\ mg^{-1}$	10.16	[11]
CoP hollow nanocage	1.0 M KOH	Indophenol blue method	-0.4	10.78 $\mu g\ h^{-1}\ mg^{-1}$	7.36	[12]
α-Fe nanorods	[C4mpyr][eFAP]	Indophenol blue method	-0.23	2.35×10^{-11} mol $s^{-1}\ cm^{-2}$	32	[13]
Mo_2C/C	0.5 M Li_2SO_4	Nessler's reagent method	-0.3	11.3 $\mu g\ h^{-1}\ mg^{-1}$	7.8	[14]
$Ti_3C_2T_x$-MXene	0.5 M Li_2SO_4	Nessler's reagent method	-0.1	4.7 $\mu g\ cm^{-2}\ h^{-1}$	5.78	[15]
B_4C nanosheet	0.1 M HCl	Indophenol blue method	-0.75	26.57 $\mu g\ h^{-1}\ mg^{-1}$	15.95	[16]
Bi nanoparticles	0.5 M K_2SO_4	Indophenol blue method	-0.6	0.052 mmol $cm^{-2}\ h^{-1}$	66	[17]
S-doped carbon nanospheres	0.1 M Na_2SO_4	Indophenol blue method	-0.7	19.07 $\mu g\ h^{-1}\ mg^{-1}$	7.47	[18]
Fe_2O_3-CNT	0.5 M KOH	Salicylate method	-2	0.649 $\mu g\ cm^{-2}\ h^{-1}$	0.164	[19]
Fe_2O_3 nanorods	0.1 M Na_2SO_4	Indophenol blue method	-0.8	15.9 $\mu g\ h^{-1}\ mg^{-1}$	0.94	[20]
Fe/Fe_3O_4	0.1 M PBS	Indophenol blue method	-0.3	0.19 $\mu g\ cm^{-2}\ h^{-1}$	8.29	[21]
Spinel Fe_3O_4 nanorods	0.1 M Na_2SO_4	Indophenol blue method	-0.4	5.6×10^{-11} mol $s^{-1}\ cm^{-2}$	2.6	[22]
β-FeOOH nanorods	0.5 M $LiClO_4$	Indophenol blue method	-0.75	23.32 $\mu g\ h^{-1}\ mg^{-1}$	6.7	[23]
Fe_3S_4 nanosheets	0.1 M HCl	Indophenol blue method	-0.4	75.4 $\mu g\ h^{-1}\ mg^{-1}$	6.45	[24]
FeS/MoS_2	0.1 M Na_2SO_4	Indophenol blue method	-0.5	8.45 $\mu g\ cm^{-2}\ h^{-1}$	2.96	[25]
$FeMoO_4$ nanorods	0.5 M $LiClO_4$	Indophenol blue method	-0.5	45.8 $\mu g\ h^{-1}\ mg^{-1}$	13.2 (-0.3 V)	[26]
$FeMoN_6$ single atom catalyst	0.25 M $LiClO_4$	Indophenol blue method	-0.3	14.95 $\mu g\ h^{-1}\ mg^{-1}$	41.7 (-0.2 V)	[27]
Mo_3Fe_3C	1 M KOH	Indophenol blue method	-0.05	1.23 $\mu g\ h^{-1}\ mg^{-1}$	27	[28]
VN nanoparticles	Nafion	Nessler's	-0.1	3.31×10^{-10}	5.95	[29]

		reagent method		mol s^{-1} cm^{-2}		
VN nanosheets	0.1 M HCl	Indophenol blue method	-0.5	8.40×10^{-11} mol s^{-1} cm^{-2}	2.25	[30]
Hollow VO_2 microspheres	0.1 M Na_2SO_4	Indophenol blue method	-0.7	21.4 μg h^{-1} mg^{-1}	3.97	[31]
V_2O_3/C	0.1 M Na_2SO_4	Indophenol blue method	-0.6	12.3 μg h^{-1} mg^{-1}	7.28	[32]
$FeVO_4$ PNRs	0.5 M $LiClO_4$	Indophenol blue method	-0.4	52.8 μg h^{-1} mg^{-1}	15.7	This work

Supplementary references

[1] B. Hu, M. Hu, L.C. Seefeldt, T.L. Liu, ACS Energy Lett. 4 (2019) 1053-1054.

[2] K. Chu, J. Wang, Y.P. Liu, Q.Q. Li, Y.L. Guo, J. Mater. Chem. A 8 (2020) 7117-7124.

[3] K. Chu, Y. Liu, Y. Chen, Q. Li, J. Mater. Chem. A 8 (2020) 5200-5208.

[4] K. Chu, Q. Li, Y. Liu, J. Wang, Y. Cheng, Appl. Catal. B 267 (2020) 118693.

[5] D. Zhu, L. Zhang, R.E. Ruther, R.J. Hamers, Nat. Mater. 12 (2013) 836.

[6] G.W. Watt, J.D. Chrisp, Anal. Chem. 24 (1952) 2006-2008.

[7] S.J. Clark, M.D. Segall, C.J. Pickard, P.J. Hasnip, M.I.J. Probert, K. Refson, M.C. Payne, Z. Kristallogr. 220 (2005) 567-570.

[8] V.I. Anisimov, F. Aryasetiawan, A. Lichtenstein, J. Phys.- Condens. Mat. 9 (1997) 767.

[9] A.A. Peterson, Energy Environ. Sci. 3 (2010) 1311-1315.

[10] W. Wang, Y. Zhang, X. Huang, Y. Bi, J. Mater. Chem. A 7 (2019) 10949-10953.

[11] C. Lv, C. Yan, G. Chen, Y. Ding, J. Sun, Y. Zhou, G. Yu, Angew. Chem. Int. Edit. 130 (2018) 6181-6184.

[12] W. Guo, Z. Liang, J. Zhao, B. Zhu, K. Cai, R. Zou, Q. Xu, Small Methods 2 (2018) 1800204.

[13] B.H. Suryanto, C.S. Kang, D. Wang, C. Xiao, F. Zhou, L.M. Azofra, L. Cavallo, X. Zhang, D.R. MacFarlane, ACS Energy Lett. 3 (2018) 1219-1224.

[14] H. Cheng, L.X. Ding, G.F. Chen, L. Zhang, J. Xue, H. Wang, Adv. Mater. 30 (2018) 1803694.

[15] Y.R. Luo, G.F. Chen, L. Ding, X.Z. Chen, L.X. Ding, H.H. Wang, Joule 3 (2019) 279-289.

[16] W. Qiu, X.-Y. Xie, J. Qiu, W.-H. Fang, R. Liang, X. Ren, X. Ji, G. Cui, A.M. Asiri, G. Cui, Nat. Commun. 9 (2018) 3485.

[17] Y.-C. Hao, Y. Guo, L.-W. Chen, M. Shu, X.-Y. Wang, T.-A. Bu, W.-Y. Gao, N. Zhang, X. Su, X. Feng, J.-W. Zhou, B. Wang, C.-W. Hu, A.-X. Yin, R. Si, Y.-W. Zhang, C.-H. Yan, Nat. Catal. 2 (2019) 448-456.

[18] L. Xia, X. Wu, Y. Wang, Z. Niu, Q. Liu, T. Li, X. Shi, A.M. Asiri, X. Sun, Small Methods 3 (2018) 1800251.

[19] S. Chen, S. Perathoner, C. Ampelli, C. Mebrahtu, D. Su, G. Centi, Angew. Chem. Int. Edit. 56 (2017) 2699-2703.

[20] X. Xiang, Z. Wang, X. Shi, M. Fan, X. Sun, ChemCatChem 10 (2018) 4530-4535.

[21] L. Hu, A. Khaniya, J. Wang, G. Chen, W.E. Kaden, X. Feng, ACS Catal. 8 (2018) 9312-9319.

[22] Q. Liu, X. Zhang, B. Zhang, Y. Luo, G. Cui, F. Xie, X. Sun, Nanoscale 10 (2018) 14386-14389.

[23] X. Zhu, Z. Liu, Q. Liu, Y. Luo, X. Shi, A.M. Asiri, Y. Wu, X. Sun, Chem. Commun. 54 (2018) 11332-11335.

[24] X. Zhao, X. Lan, D. Yu, H. Fu, Z. Liu, T. Mu, Chem. Commun. 54 (2018) 13010-13013.

[25] Y. Guo, Z. Yao, B.J.J. Timmer, X. Sheng, L. Fan, Y. Li, F. Zhang, L. Sun, Nano Energy 62 (2019) 282-288.
[26] K. Chu, Q.Q. Li, Y.H. Cheng, Y.P. Liu, ACS Appl. Mater. Inter. 12 (2020) 11789-11796.
[27] Y. Li, Q. Zhang, C. Li, H.-N. Fan, W.-B. Luo, H.-K. Liu, S.-X. Dou, J. Mater. Chem. A 7 (2019) 22242-22247.
[28] B. Qin, Y. Li, Q. Zhang, G. Yang, H. Liang, F. Peng, Nano Energy 68 (2020) 104374.
[29] X. Yang, J. Nash, J. Anibal, M. Dunwell, S. Kattel, E. Stavitski, K. Attenkofer, J.G. Chen, Y. Yan, B. Xu, J. Am. Chem. Soc. 140 (2018) 13387-13391.
[30] R. Zhang, Y. Zhang, X. Ren, G. Cui, A.M. Asiri, B. Zheng, X. Sun, ACS Sustain. Chem. Eng. 6 (2018) 9545-9549.
[31] Q. Liu, R. Zhang, H. Guo, L. Yang, Y. Wang, Z. Niu, H. Huang, H. Chen, L. Xia, T. Li, ChemElectroChem 6 (2019) 1014-1018.
[32] R. Zhang, J. Han, B. Zheng, X. Shi, A.M. Asiri, X. Sun, Inorg. Chem. Front. 6 (2019) 391-395.